Frequency limits of terahertz radiation generated by optical-phonon transit-time resonance in quantum wells and heterolayers

P. Shiktorov, E. Starikov, and V. Gružinskis
Semiconductor Physics Institute, A. Goštauto 11, LT 01108 Vilnius, Lithuania

L. Varani, C. Palermo, and J.-F. Millithaler
Institut d'Électronique du Sud (CNRS UMR 5214), Université Montpellier 2, Place Eugène Bataillon, 34095 Montpellier Cedex 5, France

L. Reggiani
Dipartimento di Ingegneria dell'Innovazione, Università del Salento and CNISM, Via Arnesano s/n, I-73100 Lecce, Italy
(Received 14 December 2006; revised manuscript received 28 May 2007; published 25 July 2007)

We develop an analytical model based on a few generalized parameters of bulk materials and two-dimensional (2D) structures which enables us to analyze the main features of terahertz (THz) radiation generation caused by optical-phonon transit-time resonance. In the framework of such a model and direct Monte Carlo simulations it is shown that for the same material (i) generation conditions are the same in quantum wells and heterolayers characterized by the same parameter of electron localization in the 2D channel and (ii) a considerable increase up to 5 times of the high-frequency cutoff for THz radiation generation is predicted in going from 3D to 2D transport.

DOI: 10.1103/PhysRevB.76.045333 PACS number(s): 72.20.Ht, 72.30.+q, 73.63.Hs, 63.20.Kr

I. INTRODUCTION

It is well known that in most semiconductors at lattice temperatures considerably lower than the Debye temperature the occupation of momentum space by hot carriers is subdivided into two regions with respect to optical-phonon emission processess (see, e.g., Ref. 1 and references therein). The former (the so-called *passive region*) corresponds to carrier energy ϵ less than the optical phonon energy $\hbar\omega_0$. The latter (the so-called *active region*) corresponds to the opposite case $\epsilon > \hbar\omega_0$.

In the passive region, only scattering by acoustic phonons and impurities with combined characteristic time τ_- (the effective momentum relaxation) is possible. As a consequence, because of the presence of a dc electric field E, carriers can move quasiballistically in this region, the condition for such a motion being usually formulated in terms of characteristic times as

$$\tau_E \ll \tau_-. \tag{1}$$

Here $\tau_E = p_0/eE$ is the optical-phonon transit time—i.e., the time necessary for a carrier to cross the hemisphere with radius $p_0 = \hbar k_0 = \sqrt{2m^* m_0 \hbar\omega_0}$ in momentum space and to reach the optical-phonon energy, with e being the electron charge, $\hbar$ the reduced Planck constant, m_0 the free electron mass, and m^* the effective mass.

In the active region, spontaneous emission of optical phonons plays the predominant role. Accordingly, by emitting an optical phonon a carrier returns back into the passive region. When the penetration into the active region is sufficiently small,

$$\delta\epsilon = \epsilon - \hbar\omega_0 \ll \hbar\omega_0, \tag{2}$$

all the carriers move practically along the $\mathbf{p} \| \mathbf{E}$ axis from $p \approx 0$ up to $p \geqslant p_0$, periodically repeating this motion with frequency $f_E = 1/\tau_E$. In terms of the characteristic times this condition is usually formulated as

$$\tau_+ \ll \tau_E, \tag{3}$$

where τ_+ is the characteristic time of the optical-phonon emission in the active region.

Under stationary conditions, such a situation results in the Baraff-like distribution function[2] elongated in the momentum space along the electric field direction (the so-called *streaming distribution*).[1,3,4] These kinds of distributions are responsible by themselves for various mechanisms of terahertz (THz) radiation generation such as light–to–heavy-hole lasers in crossed electric and magnetic fields in p-Ge (see, e.g., the recent review in Ref. 5), negative effective mass cyclotron resonance MASER,[6] etc.

From a dynamical point of view, in such a situation the carrier motion in the passive region takes a cyclic character with transit-time frequency $f_E = 1/\tau_E$. Such a carrier dynamics originates a variety of quite important physical phenomena. For example, the transit-time frequency manifests itself in (i) dumping oscillations during a transient response of the carrier ensemble under a steplike switching of the dc electric field,[7] (ii) resonant enhancement of the current noise spectrum at frequency near to f_E,[8] (iii) a bunching of carriers in momentum space,[9–11] (iv) noise upconversion effects[12] under ac electric field, etc. Below we shall refer to such a periodic or resonant behavior as optical-phonon transit-time resonance (OPTTR).

In a set of pioneering papers,[13–16] it was predicted that by superimposing onto a high dc field a small ac field the oscillating dynamics leads to a carrier bunching in momentum space with a phase shift that can originate microwave power generation. In this case, near to the OPTTR frequency, the real part of the small-signal mobility takes negative values,

which is usually called "dynamic negative differential mobility" (DNDM). Theoretical considerations of the above predictions[13–16] stressed that DNDM at OPTTR can appear due to (i) the polarity of the optical-phonon emission under a small penetration into the active region and (ii) a decrease with electron energy increase of the scattering rate in the passive region, as takes place for impurity and piezoelectric phonon scattering [by assuming the validity of the condition given by Eq. (1)].

Monte Carlo (MC) simulations performed for bulk GaAs and InP confirmed the possibility of microwave generation with maximum frequency of about 300–400 GHz.[17–19] Such a generation was observed experimentally in InP samples by the Vorob'jev group of Saint Petersburg[20] under conditions close to those predicted by MC simulations. The success of this experimental confirmation made finding a way to extend the generation region up to the THz frequency range a major issue.

Since the OPTTR frequency $f_E = eE/p_0$ is proportional to the applied dc electric field E, to increase the generation frequency one needs to increase E. For a given material, an increase of E leads eventually to a deterioration of the OPTTR condition given by Eq. (3). Therefore, an increase of the OPTTR frequency can be expected in semiconductors with a carrier-phonon interaction stronger than in standard III-V compounds, so that the smaller values of τ_+ could be achieved. Such a requirement is satisfied by wideband nitride materials where the electron-phonon interaction is several times stronger than in standard III-V compounds. Indeed, recent MC simulations[21–23] have predicted that in III-nitride compounds the maximum generation frequency can reach values in the range 1–4 THz and that the possibility of generation can persist up to liquid nitrogen temperatures.

However, nitride materials in the form of bulk samples are practically not available at the present time. Available samples are mostly heterostructures (HSs) with two-dimensional (2D) electron transport such as quantum wells (QWs) and heterolayers (HLs). In this context, it is worthwhile to emphasize that transport in 2D exhibits two main advantages with respect to that in 3D: namely, (i) the possibility to increase the maximum generation frequency because of a more abrupt threshold of the scattering rate due to optical-phonon emission and (ii) the possibility to use high carrier densities but avoiding impurity scattering, since donors are usually remotely placed outside the 2D channel.

In terms of Eqs. (1) and (3), the former possibility improves the validation of conditions posed by Eq. (3), while the latter helps to fulfill the condition posed by Eq. (1). These circumstances have stimulated investigation of the OPTTR for the case of a 2D electron transport as was carried out in recent theoretical investigations.[24–28] For example, by using MC simulations of electron transport in 2D GaN (Refs. 26–28) and InP (Ref. 28) QWs a considerable increase of the maximum generation frequency, up to 3 times, was predicted with respect to the 3D case. Furthermore, the influence of hot-phonon effects, degeneracy, and electron-electron interactions on the OPTTR in QWs was considered in Ref. 27, where a critical influence of electron-electron scattering on the OPTTR was also pointed out. (In our opinion this influence was rather overestimated since it was based on a thermal Fermi distribution function of carriers, which does not satisfy OPTTR conditions where strong heating of the electron system characterized by streaming distributions takes place.) To summarize the state of the art, Fig. 1 reports and compares results of MC simulations of the OPTTR generation frequency band as function of the applied dc field for various 3D and 2D semiconductor structures. The low-frequency cutoff of the generation is related to violation of the quasiballistic motion of electrons in the passive region [Eq. (1)], while the high-frequency cutoff is related to the increasing penetration of electrons into the active region [Eq. (3)].

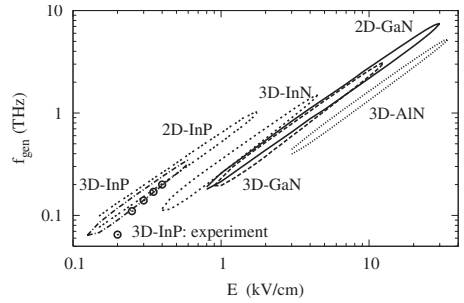

FIG. 1. Generation bands (frequency regions where the real part of the differential mobility is negative) as function of applied dc field calculated by the MC method for bulk materials (Refs. 21–23) as well as 12-nm InP (Ref. 28) and 5-nm GaN (Refs. 26 and 28) QW structures at 10 K. Points show the generation frequency obtained experimentally by Vorob'ev *et al.* (Ref. 20).

As evident from Fig. 1 the electric field regions, and hence the generation bands, cover a rather wide frequency range, which strongly depends on the semiconductor material and the transport type (2D or 3D). Such a strong dependence on material and transport type as well as on external conditions such as temperature, etc., complicates the microscopic interpretation of experiments since for each given case it is necessary to perform MC simulations of the possible generation bands, to determine the values of the amplification coefficient in the bands, etc. Additional complications appear in going from 3D to 2D transport. Primarily, they are related to the necessity to calculate the wave functions of electron states in a 2D channel in each given case and then to use them for the determination of the scattering rates.[26,27] Therefore, for a better understanding of the main tendencies and a further development of the experimental samples and techniques related to the OPTTR phenomena a unified approach able to account for the relevant parameters of the bulk material as well as for the specific parameters of an heterostructure (square or triangular barriers, quantum layer width, etc.) would be highly desirable.

The aim of this work is to address this issue by developing an analytical model of the OPTTR able to predict the main features of THz radiation generation on the basis of some generalized parameters characterizing the bulk materials and the 2D channels. In order to simplify the model, the main attention will be paid to the two phonon scattering mechanisms that, in essence, determine the conditions for the OPTTR: i.e., deformation acoustic-phonon scattering in the passive region and polar optical-phonon emission in the ac-

tive region. The model does not include electron-electron, ionized impurity, and piezoelectrical scattering mechanisms since their importance becomes marginal at increasing electron energies. In any case, their influence can be taken into account when evaluating the values of τ_- that are critical for OPTTR.

II. MODEL

To compare the 2D transport in a QW and single-interface HL we make use of analytical expressions for the wave functions. To exclude the influence of upper minibands on the OPTTR, the energy separation between the first and second minibands is supposed to satisfy the condition

$$\Delta_{12} \equiv \frac{\epsilon_2(\mathbf{k}_\perp) - \epsilon_1(\mathbf{k}_\perp)}{\hbar\omega_0} \geqslant 1, \tag{4}$$

where $\epsilon_{1,2}$ is the carrier energy of miniband 1 and 2, respectively, and $\mathbf{k}_\perp$ the electron wave vector along the 2D layer. In such a case, under a small penetration of electrons into the active region $\epsilon_1(\mathbf{k}_\perp) > \hbar\omega_0$ all the transitions induced by scattering events occur inside the first miniband only.

For the limiting case of a deep QW and HL (the square and triangular wells, respectively) the square of the wave function modulus for the first miniband takes the form[29–31]

$$|\psi(z)|^2 = \begin{cases} \dfrac{2}{a}\sin^2\left(\dfrac{\pi}{a}z\right), & \text{QW}, \\ \dfrac{1}{2}b^3 z^2 \exp(-bz), & \text{HL}, \end{cases} \tag{5}$$

where z is the coordinate in the direction normal to the interface, a the width of the QW, and the coefficient b of the Fang-Howard-Stern wave function is usually related to the sheet carrier density n as[29] (for simplicity we omit the depletion charge in the HL)

$$b^3 = \frac{33 m_0 m^* e^2}{8\kappa_0\kappa_s\hbar^2} n, \tag{6}$$

with κ_0 and κ_s being the vacuum permittivity and the static dielectric constant of the material, respectively.

To characterize the 2D transport properties of a QW and HL in terms of unified quantities we define an effective width of the electron localization in a 2D channel in the direction of the quantitization d as

$$d^{-1} = \int |\psi(z)|^4 dz. \tag{7}$$

We note that, by introducing this parameter, Price[29–31] included an additional factor 1/2 which is here omitted since in the case of plane waves $\psi \sim \frac{1}{\sqrt{L}}\exp(ikz)$ the effective width defined by Eq. (7), $d=L$, coincides entirely with the wave-function localization inside a box. For the wave functions given in Eq. (5) one obtains

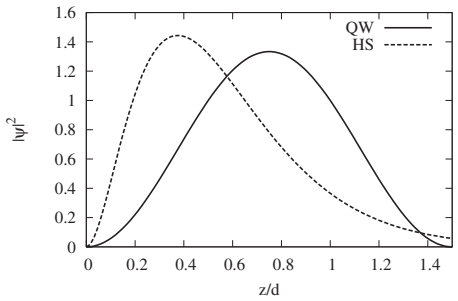

FIG. 2. Square of the wave function $\psi(z)$ for the normal-direction quantitization of the lowest electron state in a QW and a HL (solid and dashed lines, respectively) as a function of the dimensionless length z/d with d being the effective width of the electron localization in a 2D channel defined by Eq. (7).

$$d = \frac{2}{3}\begin{cases} a, & \text{QW}, \\ 8/b, & \text{HL}. \end{cases} \tag{8}$$

In the following we shall represent the wave functions in QWs and HLs as functions determined by a value of the effective width d of 2D channel. By using Eq. (8), Eq. (5) can be rewritten as

$$|\psi(z)|^2 = \begin{cases} \dfrac{4}{3d}\sin^2\left(\dfrac{2\pi}{3d}z\right), & \text{QW}, \\ \dfrac{1}{2}\left(\dfrac{16}{3d}\right)^3 z^2 \exp\left(-\dfrac{16}{3d}z\right), & \text{HL}. \end{cases} \tag{9}$$

Figure 2 reports the square of the wave functions for a QW and a HL with the same localization width d as function of the dimensionless variable z/d.

To compare various semiconductors with different values of the main parameters (carrier effective mass, phonon energy, etc.) in both 2D and 3D cases it is convenient to use the momentum $\mathbf{q}=\mathbf{k}/k_0$ and energy $\varepsilon(\mathbf{q})=\epsilon(\mathbf{k})/\hbar\omega_0$ normalized to the passive area values. This normalization allows us to represent the usual scattering rates[29,30] for deformation acoustic-phonon (DA) and polar optical-phonon emission (PO) in the factorized form

$$\lambda_j^i = \Lambda_j G_j^i(\mathbf{q},\mathbf{q}'), \tag{10}$$

where the subindex $j=\text{DA},\text{PO}$ labels the scattering mechanism while superindex $i=\text{2D},\text{3D}$ labels the dimensional type of electron transport. The part of the scattering rate which is independent of the transport type (2D or 3D) is determined by the constant Λ_j as

$$\Lambda_{\text{DA}} = \frac{k_B T_0 D^2 m_0 m^*}{\pi\rho s^2\hbar^4}\hbar k_0, \tag{11}$$

$$\Lambda_{\text{PO}} = \frac{e^2(\hbar\omega_0 2m_0 m^*)^{1/2}}{4\pi\hbar^2\kappa_0}\left[\frac{1}{\kappa_\infty} - \frac{1}{\kappa_s}\right], \tag{12}$$

which depends on the usual parameters of DA and PO scattering:[29,30] namely, the Boltzmann constant k_B, the lattice temperature T_0, the deformation potential D, the material density ρ, the sound velocity s, the optical dielectric constant κ_∞, and other parameters defined above.

The dimensionless factor $G^i(\mathbf{q},\mathbf{q}')$ in Eq. (10) contains the matrix-element-induced dependence of the transition rate per unit time on electron momentum before and after the scattering event, $\mathbf{q}$ and $\mathbf{q}'$, respectively, and on the transport type (2D or 3D), which comes mainly from the energy dependence of the density of state. The DA- and PO-scattering factor G takes, respectively, the form

$$G^i_{\mathrm{DA}}(\mathbf{q},\mathbf{q}') = \begin{cases} \sqrt{\varepsilon}, & i = 3\mathrm{D}, \\ \pi/k_0 d, & i = 2\mathrm{D}, \end{cases} \tag{13}$$

and

$$G^i_{\mathrm{PO}}(\mathbf{q},\mathbf{q}') = \begin{cases} \dfrac{1}{\sqrt{\varepsilon}} \ln\left|\sqrt{\varepsilon} + \sqrt{\varepsilon'}\right| \sim \sqrt{\varepsilon - 1}, & i = 3\mathrm{D}, \\ \displaystyle\int_0^{\pi} d\phi H(u)/2Q, & i = 2\mathrm{D}, \end{cases} \tag{14}$$

where

$$u = \frac{3}{2} Q k_0 d \tag{15}$$

is a dimensionless variable,

$$Q = |\mathbf{q} - \mathbf{q}'| = \sqrt{\varepsilon + \varepsilon' - 2\sqrt{\varepsilon\varepsilon'}\cos\phi} \tag{16}$$

is the normalized phonon wave vector between the initial $\mathbf{q}$ and final $\mathbf{q}'$ states for a scattering event, ϕ is the scattering angle. The function $H(u)$ is given by usual expression[29,30]

$$H(u) = \int\int |\psi(z)|^2 |\psi(z')|^2 \exp(-k_0 Q|z - z'|) dz dz'. \tag{17}$$

By substituting Eq. (9) into Eq. (17) one obtains[29,30] analytical expressions for $H(u)$ in QWs and HLs, respectively:

$$H^{\mathrm{QW}}(u) = \frac{1}{u^2 + 4\pi^2}\left[3u + \frac{8\pi^2}{u} + \frac{32\pi^4}{u^2(u^2 + 4\pi^2)}(e^{-u} - 1)\right], \tag{18}$$

$$H^{\mathrm{HL}}(u) = \frac{512 + 72u + 3u^2}{(8 + u)^3}. \tag{19}$$

Figure 3 shows $H(u)$ as a function of the dimensionless variable u. Here, the behavior of the factor $H(u)$ in QWs and HLs is found to be practically the same. Since the forward directionality of optical-phonon scattering (i.e., the preference to keep the same direction for the momentum before and after a scattering event) is determined by the angular dependence $H[u(\phi)]$,[32] we conclude that it is practically the same for the QW and HL with the same localization parameter d.

As follows from Eqs. (13) and (14) the intensities of phonon scatterings in 3D and 2D cases differ in two main aspects.

First, in the 2D cases for both QWs and HLs the DA- and PO-phonon-scattering rates are determined by an effective width of the quantum structure described by the same dimensionless parameter $k_0 d$. For the DA-phonon scattering, the intensity grows with the decrease of $k_0 d$ as $G^{\mathrm{2D}}_{\mathrm{DA}} \sim 1/(k_0 d)$. By contrast, for the PO scattering the intensity tends to saturate $G^{\mathrm{2D}}_{\mathrm{PO}} \to \pi/2$. With the decrease of the effective width $k_0 d$, there appears a significant increase of the DA-scattering rate inside the passive region, which leads to the deterioration of the OPTTR realization conditions in weak electric fields [see Eq. (4)]. Therefore, the use of wide QWs or HLs is restricted by Eq. (4), which allows us to estimate the maximum width of quantum structures when the upper miniband has no influence on the OPTTR. For example, in the case of QWs the energy separation is given by

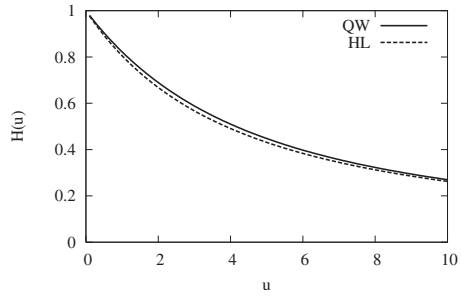

FIG. 3. Factor $H(u)$ calculated by using Eqs. (18) and (19) in QW and HL, respectively, as function of the dimensionless momentum transfer u defined by Eq. (15).

$$\Delta^{\mathrm{QW}}_{12} = \frac{4}{3}\frac{\pi^2}{(k_0 d)^2}. \tag{20}$$

By using Eq. (4) this gives us an optimum value $k_0 d = 2\pi/\sqrt{3}$, when the DA-phonon scattering in the passive region is minimum under the constraint that the upper miniband still has no effect on OPTTR. Figure 4 shows the maximum values of DA- and PO-phonon-scattering rates [$G^{\mathrm{2D}}_{\mathrm{DA}}(\varepsilon=0)$ and $G^{\mathrm{2D}}_{\mathrm{PO}}(\varepsilon=1)$, respectively] as functions of Δ_{12} related to the effective width as $k_0 d = 2\pi/\sqrt{3\Delta_{12}}$ in the QW case.

The second significant difference between 3D and 2D cases comes from the difference in the energy dependence of the final density of states. This is illustrated in Fig. 5, which compares DA- and PO-scattering rates for a 2D GaN QW with $a=5$ nm and for a homogeneous 3D GaN. In the 3D

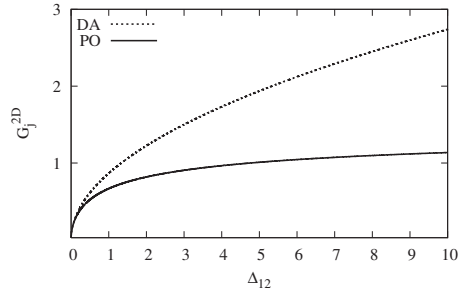

FIG. 4. Dimensionless parameter of the Da and Po scatterings as a function of the energy gap between the second and first miniband, Δ_{12}, defined for QWs by Eq. (20).

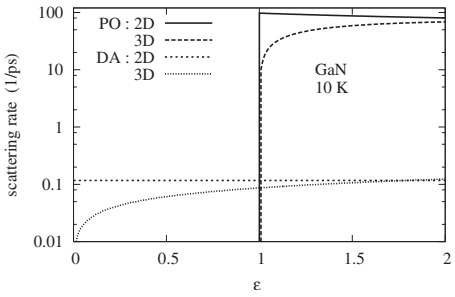

FIG. 5. Scattering rates for polar-optical-phonon emission (PO) and deformation acoustic (DA) scatterings in bulk GaN (3D) and 5-nm GaN QW (2D) as functions of the electron energy $\varepsilon(\mathbf{q}) = \epsilon(\mathbf{k})/\hbar\omega_0$ normalized to the optical-phonon energy $\hbar\omega_0$.

case the density of final states yields the square-root dependence of the scattering intensity on the carrier energy for both the DA- and PO-scattering mechanisms, $\sqrt{\varepsilon}$ and $\sqrt{\varepsilon-1}$, respectively. By contrast, for the 2D transport, the density of final states exhibits a steplike dependence on the carrier energy. Such a difference for the scattering rate of 3D and 2D transport influences essentially the scattering intensity in both the passive and active regions. This, in turn, will act on the satisfaction of the conditions for both low- and high-frequency cutoff of the OPTTR given by Eqs. (1) and (3), respectively.

The low-frequency cutoff. MC calculations show that the low-frequency cutoff of the DNDM at OPTTR takes place when the average momentum relaxation rate in the passive region $1/\tau_-$, which includes all the scatterings, increases up to critical values comparable with the transit-time frequency f_E:

$$\frac{1}{\tau_-^i} \sim f_E \begin{cases} 1/2, & i = 3\mathrm{D}, \\ 1, & i = 2\mathrm{D}. \end{cases} \tag{21}$$

We stress that Eq. (21) details numerically the qualitative condition formulated by Eq. (1). As follows from Eq. (21), the condition for the low-frequency cutoff in the 2D case is weaker than that in 3D case at least for a factor of 2. This result is connected with the fact that the probability to lose entirely the longitudinal momentum during a single-scattering event—i.e., the probability for an electron to be scattered with a change of the momentum direction by an angle $\pi/2$—in the 3D case is two times higher than that in the 2D case. Such a change represents the worst transition for the achievement of a streaming dynamics and effectively destroys the periodicity of the optical-phonon emission necessary for the OPTTR.

Let us compare the critical values of τ_-^i obtained by MC simulations [see Eq. (21)] with analytical predictions based on Eqs. (10) and (13). For simplicity we shall assume that in the passive region all the electrons move in the neighborhood of the so-called main trajectory, which starts at $\varepsilon=0$ and ends at the optical-phonon sphere $\varepsilon=1$. In this case, the evaluation of the average intensity of DA scattering, $\langle \nu_{\mathrm{DA}} \rangle$, is obtained in accordance with

$$\langle \nu_{\mathrm{DA}}^i \rangle = \frac{1}{\tau_E} \int_0^{\tau_E} \lambda_{\mathrm{DA}}^i [\varepsilon(t')] dt', \tag{22}$$

where the time dependence of the electron energy on the main trajectory takes the form

$$\varepsilon(t) = \left(\frac{t}{\tau_E} \right)^2. \tag{23}$$

By substituting into Eq. (22) the energy dependence of the DA-scattering intensity given by Eqs. (10) and (13) one obtains

$$\langle \nu_{\mathrm{DA}}^i \rangle = \Lambda_{\mathrm{DA}} \begin{cases} 1/2, & i = 3\mathrm{D}, \\ \pi/k_0 d, & i = 2\mathrm{D}. \end{cases} \tag{24}$$

By assuming that $\tau_-^i = \langle \nu_{\mathrm{DA}}^i \rangle^{-1}$ and combining Eqs. (21) and (24) one obtains the ratio between the low-frequency cutoff in 2D and 3D cases:

$$\frac{f_{\mathrm{cut}}^{2\mathrm{D}}}{f_{\mathrm{cut}}^{3\mathrm{D}}} = \frac{\pi}{k_0 d}. \tag{25}$$

As follows from Eq. (25), with the decrease of the effective width $k_0 d$ the low-frequency cutoff in the 2D case will shift to the region of higher frequencies with respect to the 3D case. However, at the optimum value $k_0 d = 2\pi/\sqrt{3}$ for QWs, when $\Delta_{12}=1$, the low-frequency cutoff caused by DA-scattering in 2D practically coincides with that in 3D, indeed $f_{\mathrm{cut}}^{2\mathrm{D}}/f_{\mathrm{cut}}^{3\mathrm{D}} \approx 0.9$.

The high-frequency cutoff. The presence of the steplike onset of the PO-scattering in the 2D case leads to a significant decrease of the electron penetration into the active region under the same electric field E as in the 3D case. In essence, such a decrease of penetration means an extension to higher values of the electric field range for the OPTTR DNDM realization, thus increasing the high-frequency cutoff of THz generation.

MC calculations show that the upper cutoff frequency for generation by OPTTR is related to a critical depth of carrier penetration into the active region $\varepsilon(\mathbf{q}) > 1$. Independently of 3D or 2D transport type, the cutoff appears at the same value of the average penetration depth:

$$\langle \delta\varepsilon \rangle_{\mathrm{cut}} \approx 0.14 - 0.15. \tag{26}$$

Again, analogously with Eq. (21), the condition given by Eq. (26) can be treated as the quantitative evaluation of the qualitative restrictions given by Eqs. (2) and (3). This allows us to estimate the maximum generation frequency caused by the OPTTR by comparing the above value with analytical predictions.

To estimate the dependence on the applied electric field strength E of the average penetration depth in 3D and 2D cases, we shall apply the procedure to determine the free-flight time $\tilde{\tau}$ in the active region used in the framework of the MC approach[33]:

$$\int_0^{\tilde{\tau}} \lambda_{\mathrm{PO}}^i[k_+(t')]dt' = -\ln(r). \tag{27}$$

Here at $t'=0$ the electron is placed at the boundary of the active region—i.e., $k_+(t')=k_0+eEt'/\hbar$, where r is a random number uniformly distributed in the interval [0,1]. Under a small depth of carrier penetration into the active region, the following approximation of the PO-phonon emission can be used for 3D and 2D cases, respectively:

$$\lambda_{\mathrm{PO}}^i = \Lambda_{\mathrm{PO}} \begin{cases} \sqrt{\varepsilon - 1}, & i = 3\mathrm{D}, \\ G_{\mathrm{PO}}^{2\mathrm{D}}(\varepsilon = 1), & i = 2\mathrm{D}. \end{cases} \tag{28}$$

By substituting Eq. (28) into Eq. (27), taking into account that the penetration depth into the active region $\delta\varepsilon=\varepsilon[k(t)]-1$ is related to the free-flight time $\tilde{\tau}$ by the simple relation

$$\delta\varepsilon \approx \frac{2eE}{\hbar k_0}\tilde{\tau} = 2\frac{\tilde{\tau}}{\tau_E}, \tag{29}$$

after averaging over the random number r one obtains the characteristic time of optical-phonon emission in the active region:

$$\tau_+^i = \langle\tilde{\tau}\rangle = \begin{cases} (\hbar k_0/2eE_{\mathrm{PO}}^{3\mathrm{D}})(9E_{\mathrm{PO}}^{3\mathrm{D}}/E)^{1/3}\Gamma(5/3), & 3\mathrm{D}, \\ \hbar k_0/eE_{\mathrm{PO}}^{2\mathrm{D}}, & 2\mathrm{D}, \end{cases} \tag{30}$$

where

$$E_{\mathrm{PO}}^i = \begin{cases} \hbar k_0 \Lambda_{\mathrm{PO}}/e, & i = 3\mathrm{D}, \\ E_{\mathrm{PO}}^{3\mathrm{D}} G_{\mathrm{PO}}^{2\mathrm{D}}(\varepsilon = 1), & i = 2\mathrm{D}, \end{cases} \tag{31}$$

is the effective electric field characterizing the intensity of optical-phonon scattering in the 3D and 2D cases, respectively, and $\Gamma(z)=\int_0^\infty t^{z-1}e^{-t}dt$ is the Γ function. As follows from Eq. (30), in the 2D case τ_+ is independent of the applied field E, while in the 3D case it decreases with an increase of E. The average depth of the electron penetration into the active region is obtained by substituting Eq. (30) into Eq. (29):

$$\langle\delta\varepsilon\rangle^i = \begin{cases} \Gamma(5/3)(3E/E_{\mathrm{PO}}^{3\mathrm{D}})^{2/3}, & i = 3\mathrm{D}, \\ 2E/E_{\mathrm{PO}}^{2\mathrm{D}}, & i = 2\mathrm{D}. \end{cases} \tag{32}$$

Since the high-frequency cutoff of the DNDM, in both the 2D and 3D cases, takes place at the same value of electron penetration into the active region, $\langle\delta\varepsilon\rangle^i=\langle\delta\varepsilon\rangle_{\mathrm{cut}}$, from Eq. (32) we obtain the maximum dc electric field that is necessary for the DNDM existence, E_{cut}^i. This, in turn, allows us to write a universal estimate of the ratio between the high-frequency cutoff of generation in the 2D and 3D cases as

$$\frac{f_{\mathrm{cut}}^{2\mathrm{D}}}{f_{\mathrm{cut}}^{3\mathrm{D}}} \equiv \frac{E_{\mathrm{cut}}^{2\mathrm{D}}}{E_{\mathrm{cut}}^{3\mathrm{D}}} = \frac{3}{2}\Gamma(5/3)^{3/2} \left.\frac{G_{\mathrm{PO}}^{2\mathrm{D}}(\varepsilon = 1)}{\sqrt{\langle\delta\varepsilon\rangle_{\mathrm{cut}}}} \approx 5\right|_{k_0 d \to 0}. \tag{33}$$

From Eq. (33) we conclude that the transition from 3D to 2D transport in QWs allows one to extend the upper generation frequency of the OPTTR effect up to a factor of 5. Such a gain of the maximum generation frequency in the 2D case is caused mainly by the transition from a square-root to a step-like dependence of the density of states upon carrier energy. The latter dependence reduces considerably the carrier penetration into the active region at a given E.

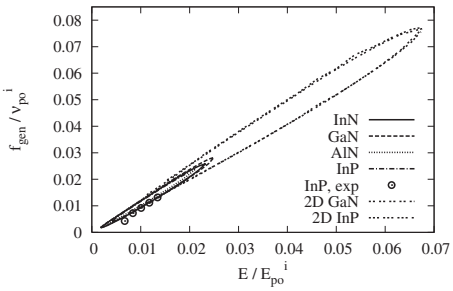

FIG. 6. Contour plot of the dynamic negative differential mobility in the E-f plane for bulk materials including experimental data (Ref. 20) for InP and 2D GaN (5-nm) and InP (12-nm) QWs. Both electric field and generation frequency values are normalized to characteristic Po-scattering fields E_{Po}^i and frequency ν_{Po}^i defined by Eqs. (31) and (34), respectively.

The universal representation of the generation band associated with OPTTR obtained for different semiconductor materials and geometry is illustrated in Fig. 6. Here the results of available calculations and experiments for various bulk materials and 2D structures already shown in Fig. 1 are presented as universal material-independent generation bands when the electric field E and the generation frequency f_{gen} are normalized, respectively, to the effective electric field E_{PO}^i defind by Eq. (31) and the effective scattering rate

$$\nu_{\mathrm{PO}}^i = eE_{\mathrm{PO}}^i/\hbar k_0 \tag{34}$$

for the PO scattering.

In the 2D case the calculations presented in Figs. 1 and 6 were performed for a value $k_0 d \approx 3.5$ which is an optimum value for the minimization of acoustic scattering in the passive region when the low-frequency cutoff is practically the same as in the 3D case. Under these conditions, $G_{\mathrm{PO}}^{2\mathrm{D}} \approx 0.8$ which from Fig. 6 gives an about 3 times increase of the high-frequency cutoff of the generation band caused by the OPTTR DNDM when going from the 3D to 2D case. By decreasing $k_0 d$ we slightly increase the high-frequency cutoff up to a factor of 5 times. However, in so doing, the low-frequency cutoff is shifted significantly to a higher-frequency region.

Such an increase of the high-frequency cutoff in 2D case means, in essence, a possibility to soften considerably the OPTTR realization critical factors related with the lattice temperature, impurity concentration, etc., by increasing the dc electric field. This is very important for the OPTTR-assisted generation mechanisms in micron and submicron n^+nn^+ 3D structures[34,35] where due to OPTTR interaction with plasma oscillations the conditions for THz generation are more soft than those in 3D homogeneous situation. For example, in InN n^+nn^+ structures the THz generation can persist up to temperatures of about 100–140 K.[34,35] For such structures the transition to 2D transport could lead to an additional extenstion of the temperature range up to room temperature.

III. CONCLUSIONS

A universal description of the OPTTR-assisted generation band of THz radiation is developed in the framework of a 3D transport in bulk materials and 2D transport in QWs and HLs. On the one hand, in the framework of an ideal streaming motion we have carried out an analytical investigation based on phonon scattering rates: namely, elastic deformation acoustic phonons in the passive energy region below the optical-phonon energy $\hbar\omega_0$ and emission of polar optical phonons in the active energy region, $\epsilon > \hbar\omega_0$. On the another hand, quantitative estimations of the qualitative constraints given by Eqs. (1) and (2) for the streaming conditions are obtained on the basis of numerical calculations of the OPTTR DNDM by the Monte Carlo method. It is found that (i) for Eq. (1) the average momentum relaxation time in the passive region must satisfy the condition $\tau_- \leqslant (1-2)\tau_E$ and (ii) for Eq. (2) carrier penetration into the active region must occurr at a level less than 14%–15%.

In the framework of such a model we have provided simple analytical expressions that estimate the low- and high-frequency limits of the generation band determined by, respectively, the average relaxation time τ_- [see Eq. (25)] and the carrier penetration into the active region [see Eq. (33)].

Having in mind that for THz radiation generation the high-frequency limit is of the most interest, for the high-frequency cutoff of the DNDM we have found that (i) for 3D bulk materials the relevant physical quantities are the carrier effective mass, the optical-phonon energy, and the polar-optical coupling strength; (ii) in passing from 3D to 2D vertical transport, for the same material the influence of 2D transport on the OPTTR is characterized entirely by the dimensionless parameter $k_0 d$ related to both the radius of the optical-phonon sphere in wave-vector space k_0 and the effective width of the electron localization d associated with the lowest miniband of the QW/HL structure; (iii) in going from 3D to 2D transport, the change of the energy dependence of the density of states is responsible for an extension of the maximum generation frequency for up to a factor of 5 times.

In essence, such a model gives the "upper" estimation of the generation band limits determined primarily by the parameters of a bulk material and a 2D structure. Any other scatterings not incorporated directly into our model—namely, impurity, electron-electron, interface roughness, etc.—act mainly on the low-frequency limit (since one can speak about the upper limit only in the case when an electron runaway from the regime of low-energy scatterings in the passive region takes place). Of course, the presence of additional low-energy scatterings will increase the low-frequency limit and eventually destroy the generation (see, e.g., Refs. 27 and 36). Nevertheless, additional scattering mechanisms can be simply incorporated into the model by taking into account their contribution to the average momentum relaxation time in the passive region τ_- as $1/\tau_- = 1/\tau_{\mathrm{DA}} + 1/\tau_{\mathrm{imp}} + 1/\tau_{ee}$. For example, such a procedure was used to estimate τ_- in the experimental observation of the OPTTR generation in bulk InP.[20] These estimations give $\tau_- \approx \tau_E$, which is reasonably close to the values estimated above.

ACKNOWLEDGMENTS

The authors acknowledge the financial support of French CNRS and Italian CNISM for a temporary position of visiting reseachers.

[1] *Far-infrared Semiconductor Lasers*, edited by E. Gornik and A. A. Andronov [Opt. Quantum Electron. **23**, S111 (1991)].
[2] G. A. Baraff, Phys. Rev. **128**, 2507 (1962).
[3] I. I. Vosilius and I. B. Levinson, Sov. Phys. JETP **23**, 1104 (1966); **25**, 672 (1967).
[4] S. Komiyama, Adv. Phys. **31**, 255 (1982).
[5] H. W. Hubers, S. G. Pavlov, and V. N. Shastin, Semicond. Sci. Technol. **20**, S211 (2005).
[6] V. I. Gavrilenko and Z. F. Krasil'nik, Opt. Quantum Electron. **23**, S323 (1991).
[7] A. Matulionis, J. Pozhela, and A. Reklaitis, Phys. Status Solidi A **31**, 83 (1975).
[8] V. Bareikis, A. Galdikas, R. Miliushyte, J. Pozhela, and V. Viktoravichius, J. Phys. (Paris), Colloq. **42**, C7-215 (1981).
[9] P. N. Shiktorov, Sov. Phys. Collect. **25**, 59 (1985).
[10] T. Kurosawa and Y. Kosano, Jpn. J. Appl. Phys., Part 1 **58**, 4104 (1989).
[11] N. Ishida and T. Kurosawa, Jpn. J. Appl. Phys., Part 1 **64**, 2994 (1995).
[12] P. Shiktorov, E. Starikov, V. Gružinskis, S. Pérez, T. González, L. Reggiani, L. Varani, and J. C. Vaissière, Phys. Rev. B **67**, 165201 (2003).
[13] V. L. Bonch-Bruevich and M. A. El-Shamuby, Vestn. Mosk. Univ., Fiz., Astron. **13**, 616 (1972).
[14] A. A. Andronov and V. A. Kozlov, JETP Lett. **17**, 87 (1973).
[15] Yu. V. Gulyaev and I. I. Chusov, Fiz. Tverd. Tela (Leningrad) **20**, 2637 (1978).
[16] A. Matulis and A. Chenis, Sov. Phys. JETP **50**, 572 (1979).
[17] E. V. Starikov and P. N. Shiktorov, Sov. Phys. Semicond. **17**, 1355 (1983).
[18] Yu. K. Pozhela, E. V. Starikov, and P. N. Shiktorov, Semicond. Sci. Technol. **7**, B386 (1992).
[19] E. V. Starikov and P. N. Shiktorov, Lietuvos Fizikos Rinkinis **32**, 471 (1992).
[20] L. E. Vorob'ev, S. N. Danilov, V. N. Tulupenko, and D. A. Firsov, JETP Lett. **73**, 219 (2001).
[21] E. Starikov, P. Shiktorov, V. Gružinskis, L. Reggiani, L. Varani, J. C. Vaissière, and Jian H. Zhao, J. Appl. Phys. **89**, 1161 (2001).
[22] E. Starikov, P. Shiktorov, V. Gružinskis, L. Reggiani, L. Varani, J. C. Vaissière, and Jian H. Zhao, IEEE Trans. Electron Devices **48**, 438 (2001).
[23] E. Starikov, P. Shiktorov, V. Gružinskis, L. Reggiani, L. Varani, J. C. Vaissière, and Jian H. Zhao, J. Phys.: Condens. Matter **13**, 7159 (2001).
[24] V. V. Korotyeyev, V. A. Kochelap, K. W. Kim, and D. L. Woolard, Appl. Phys. Lett. **82**, 2643 (2003).

[25] K. W. Kim, V. V. Korotyeyev, V. A. Kochelap, A. A. Klimov, and D. L. Woolard, J. Appl. Phys. **96**, 6488 (2004).
[26] J. T. Lu and J. C. Cao, Semicond. Sci. Technol. **20**, 829 (2005).
[27] J. T. Lu, J. C. Cao, and S. L. Feng, Phys. Rev. B **73**, 195326 (2006).
[28] E. Starikov, P. Shiktorov, V. Gružinskis, A. Dubinov, V. Aleshkin, L. Varani, C. Palermo, and L. Reggiani, J. Comput. Electron. (to be published).
[29] P. J. Price, Ann. Phys. (N.Y.) **133**, 217 (1981).
[30] P. J. Price, Phys. Rev. B **30**, 2234 (1984).
[31] P. J. Price, Surf. Sci. **143**, 145 (1984).
[32] T.-H. Yu and K. F. Brennan, J. Appl. Phys. **91**, 3730 (2002).
[33] W. Fawcett, A. D. Boardman, and S. Swain, J. Phys. Chem. Solids **31**, 1963 (1970).
[34] E. Starikov, V. Gružinskis, and P. Shiktorov, Phys. Status Solidi A **190**, 287 (2002).
[35] V. Gružinskis, P. Shiktorov, E. Starikov, L. Reggiani, L. Varani, and J. C. Vaissière, Semicond. Sci. Technol. **19**, S173 (2004).
[36] V. M. Polyakov and F. Schiwierz, J. Appl. Phys. **100**, 103704 (2006).